# Kinetics and Thermochemistry of $SiH_3 + NO$ and $SiD_3 + NO$ Reactions: Pressure Falloff and $SiH_3$−NO Bond Energy

**Lev N. Krasnoperov***

*Department of Chemical Engineering, Chemistry and Environmental Science, New Jersey Institute of Technology, Newark, New Jersey 07102*

**Ilia J. Kalinovski,[†] Jukka T. Niiranen,[‡] and David Gutman[§]**

*Department of Chemistry, The Catholic University of America, Washington, DC 20064*

*Received: January 23, 1997; In Final Form: April 21, 1997*[⊗]

The reactions of silyl and silyl-$d_3$ radicals with nitric oxide, $SiH_3 + NO \rightarrow SiH_3NO$ (1) and $SiD_3 + NO \rightarrow SiD_3NO$ (2), have been studied using pulsed excimer laser photolysis coupled with time-resolved photoionization mass spectrometry over the temperature range 301−817 K. The rate constants were measured in the ranges $0.75 \times 10^{16} \leq [He] \leq 32.0 \times 10^{16}$ molecules cm$^{-3}$ and $301 \leq T \leq 611$ K. Both reactions are in the pressure falloff regions considerably far from the true low-pressure limit. RRKM fittings using the Troe factorization approach yielded the low-pressure limit and high-pressure limit rate constants: $k_{1,tri} = (3.12 \pm 0.12) \times 10^{-29}(T/298)^{-2.96\pm0.09}$ cm$^6$ molecule$^{-2}$ s$^{-1}$, $k_{2,tri} = (9.02 \pm 0.40) \times 10^{-29}(T/298)^{-3.36\pm0.11}$ cm$^6$ molecule$^{-2}$ s$^{-1}$, $k_{1,inf} = (3.9 \pm 1.1) \times 10^{-11}(T/298)^{-1}$ cm$^3$ molecule$^{-1}$ s$^{-1}$, and $k_{2,inf} = (5.0 \pm 1.3) \times 10^{-11}(T/298)^{-1}$ cm$^3$ molecule$^{-1}$ s$^{-1}$. Equilibrium constants were measured in the temperature range 711−817 K. The standard enthalpies of reactions 1 and 2 were determined using the third law method. The bond energies determined are $DH°_0(H_3Si-NO) = 153.7 \pm 5.7$ kJ mol$^{-1}$, $DH°_{298}(H_3Si-NO) = 158.9 \pm 5.7$ kJ mol$^{-1}$, $DH°_0(D_3Si-NO) = 156.1 \pm 5.7$ kJ mol$^{-1}$, and $DH°_{298}(D_3Si-NO) = 160.8 \pm 5.7$ kJ mol$^{-1}$. This value of $DH°_0(H_3Si-NO)$ is *ca.* 30 kJ mol$^{-1}$ higher than previous estimates. *Ab initio* structural parameters were used to calculate the thermodynamic functions of $SiH_3$, $SiD_3$, $SiH_3NO$, and $SiD_3NO$. Both the singlet and the low-lying triplet states were taken into account for the adduct molecules. The calculated thermodynamic functions were used to obtain the standard entropies of the reactions 1 and 2: $\Delta S°_{298}(rxn\ 1) = 143.1$ J mol$^{-1}$ K$^{-1}$ and $\Delta S°_{298}(rxn\ 2) = 146.0$ J mol$^{-1}$ K$^{-1}$. The rate constants of the reaction $SiH_3NO + NO \rightarrow$ products (3) were measured in the temperature range 301−611 K: $k_3 = (2.95 \pm 0.38) \times 10^{-13}(T/298)^{-1.59\pm0.29}$ cm$^3$ molecule$^{-1}$ s$^{-1}$.

## Introduction

Silicon-centered transient species are the key intermediates in the silicon and silicon-containing thin film chemical vapor deposition (CVD) processes.[1,2] CVD produced thin films of silicon nitride are used in microelectronics[3,4] as well as protective coatings.[5,6] Detailed mechanistic models of CVD processes[1,2] require knowledge of a large body of elementary gas-phase and gas−surface reaction rate constants as well as thermodynamic properties.

Direct kinetic studies of reactions of small silicon hydride radicals have been recently reviewed.[7] These studies provided a significant body of rate constant data as well as (*via* the equilibrium constant determination) the Si−H and Si−N bond energies in $SiH_4$,[8] $Si(CH_3)_3H$[9], and $Si(CH_3)_3NO$.[10]

There is significant uncertainty in the magnitude of the silicon−nitrogen bond energy in nitrososilane, $SiH_3NO$. Sugawara *et al.*[11] measured the rate constant of the elementary reaction

$$SiH_3 + NO \rightarrow SiH_3NO \qquad (1)$$

at ambient temperature and reported the third-order kinetics and the termolecular rate constant $k_1 = (8.2 \pm 0.9) \times 10^{-30}$ cm$^6$ molecule$^{-2}$ s$^{-1}$ ($N_2$, 3−11 Torr). The study by Loh and Jasinski[12] at a single buffer gas density (9.5 Torr, He) confirmed the absolute value of the rate constant of reaction 1.

In the earlier studies by Nay *et al.*[13] and Kamaratos and Lampe,[14] where NO was employed as a scavenger of silyl radicals, $SiH_3ON$ was suggested as a product of reaction 1. Silylnitrosyl, $SiH_3NO$, suggested as a product of this reaction by Sugawara *et al.*,[11] was confirmed by *ab initio* calculations of Marshall.[15]

There have been attempts to evaluate the Si−N bond energy in $SiH_3NO$ based on the absolute value of the rate constant of reaction 1.[15,16] Chasovnikov *et al.*[16] using estimated structural parameters for $SiH_3NO$ concluded that the silicon−nitrogen bond in nitrososilane is relatively weak, 134−188 kJ mol$^{-1}$. Marshall,[15] using *ab initio* structural parameters, and assuming the true low-pressure limit for the rate constant reported by Sugawara *et al.*,[11] estimated $H_3Si-NO$ intrinsic bond energy as 117 kJ mol$^{-1}$. This value substantially (*ca.* 30 kJ mol$^{-1}$) differs from the *ab initio* BAC (BAC = bond additivity corrections) value calculated by Melius and Allendorf,[10] 150 kJ mol$^{-1}$ ($DH°_{298}$). The *ab initio*−BAC result for the $Si(CH_3)_3-NO$ bond enthalpy at 298 K (191 kJ mol$^{-1}$) is, however, in excellent agreement with the experimental value (190 kJ mol$^{-1}$).[10] The controversy can be summarized as follows: either reaction 1 is in its true low-pressure limit at ambient temperature and pressures below 10 Torr and the theoretical results (*ab initio*−BAC) significantly overpredict the Si−N bond energy

[†] Current address: Department of Chemistry, University of California at Berkeley, CA 94720.

[‡] Present address: Department of Physical Chemistry, University of Helsinki, Meritullinkatu 1C, SF-00170 Helsinki, Finland.

[§] Deceased.

[⊗] Abstract published in *Advance ACS Abstracts,* June 1, 1997.

S1089-5639(97)00288-0 CCC: $14.00 © 1997 American Chemical Society

in $SiH_3NO$, or the theoretical results are correct and reaction 1 is in the pressure falloff, far from the true low-pressure limit.

For these reasons, we decided to reinvestigate the kinetics of reaction 1 over a wide range of pressures and temperatures. We also decided to confirm our findings by the additional study of $SiD_3 + NO$ (reaction 2):

$$SiD_3 + NO \rightarrow SiD_3NO \quad (2)$$

Additional kinetic information on the reaction of the adduct, $Si(CH_3)_3NO$, with nitric oxide (reaction 3) was also obtained in the course of these experiments using different experimental conditions than those used to study reactions 1 and 2:

$$SiH_3NO + NO \rightarrow \text{products} \quad (3)$$

The results of these latter experiments are also presented.

## Experimental Section

The apparatus[17] and procedures used in the rate constant and equilibrium constant measurements[10,18] have been described previously. Briefly, gas flowing through the 1.05 i.d. heatable tubular quartz reactor contained the radical precursor (see below) NO in varying amounts and an inert carrier gas (He). Reaction was initiated by pulsed, unfocused 248 nm radiation from a Lambda Physik 201 MSC laser directed along the axis of the tubular reactor. The repetition rate of the laser pulses was adjusted so that the flow velocities used ($4-6$ m $s^{-1}$) were adequate to completely replace gases in the reactor between laser pulses.

Gas emerging from a small sampling orifice in the wall of the reactor is formed into a molecular beam by a conical skimmer and analyzed continuously using photoionization quadrupole mass spectrometry. Vacuum-UV radiation from atomic resonance lamps was used for photoionization.

The experiments were done using $SiH_3I$ ($(1.7-32) \times 10^{12}$ molecules $cm^{-3}$) and $SiD_3I$ ($(10-15) \times 10^{12}$ molecules $cm^{-3}$) as the $SiH_3$ and $SiD_3$ radical precursors.[12] The quantum yield of $SiH_3$ radicals at 248 nm was measured by Loh and Jasinski as 0.2.[12]

The decay of the radicals was monitored in time-resolved experiments in the absence and presence of NO (using varied concentrations) to obtain reaction rate constants. Experiments were conducted under pseudo-first-order conditions ($[NO] \gg [SiH_3]_0$, $[SiD_3]_0$).

The initial concentrations of $SiH_3$ and $SiD_3$ were kept low ($(3.8-79) \times 10^9$ and $(25-41) \times 10^9$ molecules $cm^{-3}$, respectively) to assure that radical−radical recombination was a negligible competing process.

Under the typical experimental conditions used, the silyl radicals, $SiH_3$ and $SiD_3$, were lost only by the reactions of interest (1, 2) and by a kinetically first-order heterogeneous loss processes (4, 5):

$$SiH_3 \rightarrow \text{heterogeneous loss} \quad (4)$$

$$SiD_3 \rightarrow \text{heterogeneous loss} \quad (5)$$

At low temperatures (301−611 K), the dissociation of the adducts formed in reactions 1 and 2, $SiH_3NO$ and $SiD_3NO$, is unimportant, and the observed $SiH_3(D_3)$ decay curves are single-exponential.

Only reactions 1 and 4 (2 and 5) were responsible for the observed radical decays: $I_t(SiH_3) = I_0(SiH_3) \exp(-k't)$, where $k' = k_1[NO] + k_4$. The dependence of the measured exponential decay constant ($k'$) on the concentration of NO added yielded the rate constant $k_1$.

At higher temperatures (711−811 K) $SiH_3NO$ dissociation (reaction −1) plays a role, and additional kinetic processes involving the consumption of the adduct must be taken into account. The loss of the adduct occurs by reaction 3 as well as by a heterogeneous loss process, reaction 6:

$$SiH_3NO \rightarrow \text{heterogeneous loss} \quad (6)$$

The experimental $SiH_3$ decay is expected to be a double-exponential function in this case. A standard procedure was used to calculate the equilibrium constant from the parameters of the double-exponential function fitted to the experimentally measured $SiH_3$ and $SiD_3$ radicals temporal profiles.[19,20]

Silylic radicals have rather large wall loss rate constants ($120-300$ $s^{-1}$ in a 1.05 cm i.d. reactor) even when highly inert wall coatings, such as poly(tetrafluoroethylene) or Halocarbon Wax, are used.[10,21] In an uncoated reactor, the wall loss rate constant of silyl radicals (>1000 $s^{-1}$ [21,22]) becomes too large to permit kinetic measurements. The halogenated materials (Teflon, 852-200) and Halocarbon Wax (Halocarbon Wax Corp., Hackensack, NJ) used as coatings in previous studies are stable to 280 °C (Teflon) and could not be used in the equilibrium study. To reduce the wall loss rate constant to an acceptable level ($150-300$ $s^{-1}$ in 1.05 cm reactor), a poly(dimethylsiloxane) (PDMS) with an average molecular weight of 100 000[23] and a boron oxide coating[10] were used. A PDMS coating was used over the temperature range 300−611 K and a boron oxide coating over the 300−950 K range. Boron oxide ($B_2O_3$) is liquid at temperatures above 460 °C with a very low vapor pressure (boiling point is *ca.* 1860 °C[24]). The procedure of preparation of $B_2O_3$ coating is described elsewhere.[10] The boron oxide coating has approximately the same wall activity toward $SiH_3$ and $Si(CH_3)_3$ recombination as the coatings with the halogenated materials mentioned above but can be used at least up to 950 K. (This is the highest temperature tested in the current and previous[10] studies, the actual temperature limit for this coating is unknown.)

Most of the experiments were conducted using a 1.05 cm i.d. reactor coated with boron oxide. A few series of experiments were performed using PDMS as a wall coating in order to confirm that proper account was taken of the heterogeneous reactions.

The $SiH_3$ and $SiD_3$ radicals were detected at $m/z = 31$ and 34, respectively (parent peaks), using a Cl resonance lamp with a $CaF_2$ window as the photoionization source ($h\nu = 8.9-9.2$ eV; ionization potential of $SiH_3 = 8$ eV[25]). The products of reactions 1 and 2, $SiH_3NO$ and $SiD_3NO$, were detected at their parent peaks ($m/z = 61$ and 64, respectively), using a H resonance lamp with a $MgF_2$ window ($h\nu = 10.2$ eV; ionization potentials of $SiH_3NO$ and $SiD_3NO$ are unknown).

Helium (HP) was obtained from Matheson. Nitric oxide, obtained from Aldrich, with an initial purity 98.5%, was distilled (7−9 times) to reduce the amount of $NO_2$ to a 0.003−0.02% level. The amount of nitrogen dioxide was measured mass spectrometrically. Direct measurements of $[NO_2]$ were possible at concentrations higher than 0.01%; lower levels were determined by freezing the $NO_2$ in the flowing gas at liquid nitrogen temperature for 10 min with subsequent warming of the trap and measurement of the time-integrated ion signal of the evaporating $NO_2$.[10]

$SiH_3I$ and $SiD_3I$, courteously provided by Dr. David B. Beach (IBM, Yorktown Heights, NY), were purified by trap-to-trap vacuum distillation.

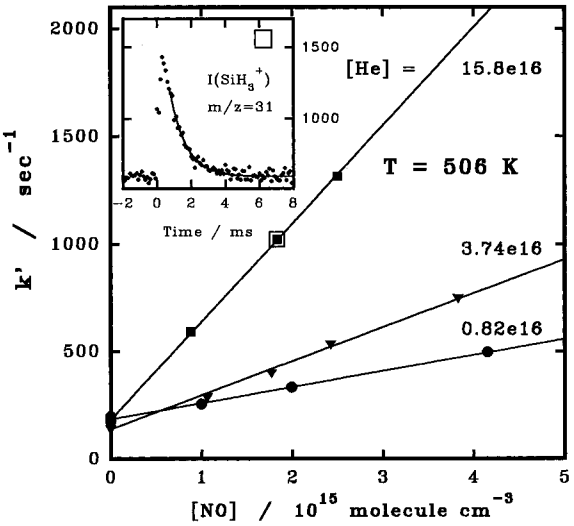


**Figure 1.** Example of silyl radical decay kinetics in the the presence of NO recorded at $m/z = 31$ (insert). The pseudo-first-order decay rate constant plotted vs NO concentration at different densities of the buffer gas (He) at $T = 506$ K. The experimental point corresponding to the displayed kinetics is indicated by the square. Experimental conditions: $[SiH_3I] = 3.15 \times 10^{13}$ molecules cm$^{-3}$, $\lambda = 248$ nm, $[He] = 15.6 \times 10^{16}$ molecules cm$^{-3}$, $[NO] = 1.86 \times 10^{15}$ molecules cm$^{-3}$, $T = 507$ K, Cl lamp with $CaF_2$ window, $B_2O_3$ wall coating.

## Experimental Results

**Kinetics and Thermochemistry of $SiH_3 + NO \rightarrow SiH_3NO$ and $SiD_3 + NO \rightarrow SiD_3NO$ Reactions.** Figure 1 displays a typical single-exponential $SiH_3$ decay profile and plots of the pseudo-first-order rate constants as a function of the concentration of added NO at different bath gas (He) densities. The slopes of the latter yield the rate constants of reaction 1. The second-order rate constants of reactions 1 and 2 obtained in this way at different densities of the bath gas (He) are shown in Figure 2. The experimental conditions of these experiments and the results obtained are given in Table 1 and Table 2. Single-exponential decays were observed up to 611 K. The rate constants obtained by the global fits of the double-exponential kinetics in the 711−817 K temperature range together with the values obtained by the extrapolation of the low-temperature data are also listed in Tables 1 and 2.

Other photolytical pathways in photodissociation of $SiH_3I$ (such as $SiH_3I + h\nu \rightarrow SiH_2 + HI$ and $SiH_3I + h\nu \rightarrow SiHI + H_2$) may lead to possible mechanistic complications. An interference of the products of these undesirable species could be expected only if the silyl radical is regenerated *via* I atom abstraction from $SiH_3I$ in secondary reactions of free radicals, or other transient species, with the precursor molecule, $SiH_3I$, on the time scale of the measurements. No explicit kinetic treatment of this problem is currently possible due to the lack of data on the products of the reactions of $SiH_2$ and SiHI with NO, as well as on the rate constants of reactions of these products with $SiH_3I$.[7] Kinetically, these processes could be revealed by varying the precursor concentration. No systematic changes of the measured rate constants with the precursor concentration have been found (see, for example, Table 1; temperature 506 ± 3 K).

Above 611 K, double-exponential decays were observed (Figure 3, insert). Double-exponential decays were recorded over the temperature range 711−817 K. At higher temperatures the lifetime of the short-lived exponent is too short and the amplitude is too small; therefore, only the lifetime of the long-lived component can be determined.

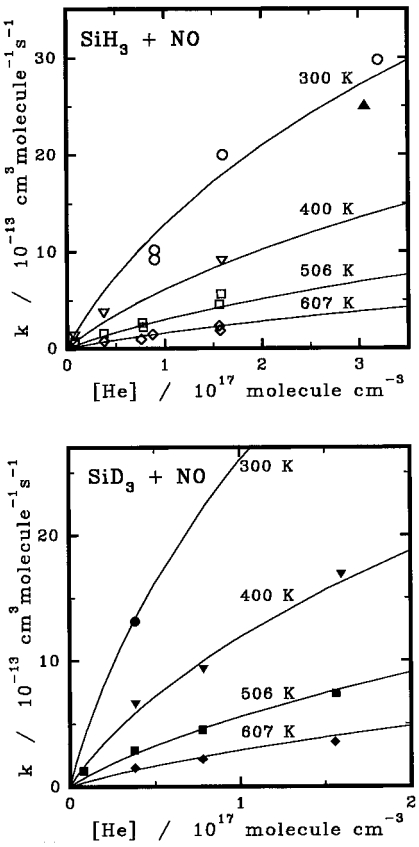


**Figure 2.** Buffer gas density dependences of the rate constants of $SiH_3 + NO \rightarrow SiH_3NO$ (top) and $SiD_3 + NO \rightarrow SiD_3NO$ (bottom) reactions at different temperatures. The solid triangle point represents the experimental result of Loh and Jasinski.[12] The solid lines drawn through the experimental points are the results of the global fits using the Troe factorization approach (see text for details).

At these higher temperatures, the mechanism of the reaction, neglecting radical−radical second-order processes, consists of the reactions 1, −1, 3, 4, and 6. The solution of the set of two linear differential equations describing this set of reactions is a double-exponential decay:[19,20]

$$[R] = [R]_0\{A_1 \exp(-\lambda_1 t) + A_2 \exp(-\lambda_2 t)\} \qquad (7)$$

The parameters of the double-exponential decay ($A_1$, $A_2$, $\lambda_1$, $\lambda_2$) are each known functions of the four combinations of the rate constants of the reactions in the mechanism and the NO concentration ($k_4$, $k_1'$, $k_{-1}$, and $k_3'$): $k_4$ is the rate constant of the radical wall loss process; $k_1' = k_1[NO]$ is the pseudo-first-order rate constant of the forward reaction 1; $k_{-1}$ is the first-order rate constant of the reverse reaction −1; $k_3' = k_3[NO] + k_6$ is the pseudo-first-order rate constant of all processes leading to disappearance of the adduct, excluding process −1. The fitting of the experimental decay curves by the double-exponential function (7) provides three parameters: $\lambda_1$, $\lambda_2$, and the ratio $A_1/A_2$. The fourth parameter, $k_4$, is determined in a separate experiment in which no NO is added. The four experimentally determined parameters were used to calculate $k_1'$, $k_{-1}$, and $k_3'$ for each experimental condition used: temperature, buffer gas density, and concentration of NO. The equilibrium constants of reaction 1 were determined using eq 8:

$$K_C = k_1/k_{-1} = (k_1'/[NO])/k_{-1} \qquad (8)$$

The equilibrium constant $K_C$ was converted into the thermodynamic equilibrium constant $K = (P_{SiH_3NO}/P^\circ)(P_{SiH_3}/P^\circ)^{-1}(P_{NO}/$

**TABLE 1: Rate Constants for $SiH_3 + NO \rightarrow SiH_3NO$**

| $T$/K[a] | [He]/$10^{16}$ [b] | [$SiH_3I$]/$10^{12}$ [b] | [$SiH_3$]$_0$/$10^9$ [b,c] | coating[d] | $k_1/10^{-13}$ [e] |
|---|---|---|---|---|---|
| 306 | 9.00 | 1.67 | 5.0 | PDMS | 10.2 ± 2.5 |
| 306 | 9.00 | 1.83 | 3.8 | PDMS | 9.20 ± 3.10 |
| 303 | 16.0 | 1.83 | 5.0 | $B_2O_3$ | 20.0 ± 3.2 |
| 301 | 32.0 | 2.40 | 5.2 | PDMS | 29.8 ± 4.2 |
| 401 | 0.748 | 26.2 | 79 | $B_2O_3$ | 1.44 ± 0.12 |
| 400 | 3.75 | 9.53 | 29 | $B_2O_3$ | 3.82 ± 0.39 |
| 397 | 15.9 | 15.6 | 47 | $B_2O_3$ | 9.19 ± 0.50 |
| 505 | 0.760 | 6.18 | 9.3 | $B_2O_3$ | 0.555 ± 0.080 |
| 505 | 0.798 | 26.6 | 80 | $B_2O_3$ | 0.704 ± 0.020 |
| 505 | 0.817 | 25.5 | 77 | $B_2O_3$ | 0.745 ± 0.027 |
| 505 | 3.74 | 25.6 | 77 | $B_2O_3$ | 1.58 ± 0.05 |
| 506 | 7.71 | 16.4 | 3.0 | $B_2O_3$ | 2.66 ± 0.08 |
| 506 | 7.80 | 9.33 | 28 | $B_2O_3$ | 2.22 ± 0.10 |
| 507 | 15.6 | 31.5 | 32 | $B_2O_3$ | 4.56 ± 0.04 |
| 507 | 15.8 | 9.27 | 28.0 | $B_2O_3$ | 5.65 ± 0.74 |
| 611 | 3.79 | 6.26 | 9.4 | $B_2O_3$ | 0.778 ± 0.032 |
| 607 | 7.58 | 4.1 | 12.0 | PDMS | 0.97 ± 0.11 |
| 608 | 8.76 | 2.23 | 6.7 | PDMS | 1.47 ± 0.15 |
| 611 | 15.6 | 3.95 | 12 | PDMS | 2.32 ± 0.23 |
| 605 | 15.7 | 6.62 | 9.9 | $B_2O_3$ | 1.86 ± 0.06 |
| From the Double-Exponential Kinetics [f] | | | | | |
| 711 | 8.77 | 1.78 | 5.3 | PDMS | 0.45 ± 0.08 (0.83)[g] |
| 715 | 15.7 | 7.05 | 10.6 | $B_2O_3$ | 1.02 ± 0.04 (1.31) |
| 730 | 30.7 | 10.6 | 111 | PDMS | 0.65 ± 0.07 (2.07) |
| 765 | 8.73 | 4.46 | 13.4 | PDMS | 0.54 ± 0.07 (0.64) |
| 769 | 15.6 | 7.05 | 10.6 | $B_2O_3$ | 0.48 ± 0.04 (1.01) |
| 812 | 3.78 | 0.87 | 1.3 | $B_2O_3$ | 0.23 ± 0.03 (0.25) |
| 817 | 15.6 | 7.14 | 10.7 | $B_2O_3$ | 0.62 ± 0.12 (0.82) |

[a] Temperature uncertainty ±3 K. [b] Concentrations in molecules $cm^{-3}$. [c] Initial concentrations of $SiH_3$ radicals calculated using the yield of $SiH_3$ in photodissociation of $SiH_3I$ at 248 nm, 0.2 (ref 12), and photodecomposition of $SiH_3I$ (typical decomposition fractions in the experiments were 1.0−1.7%, without attenuation of laser radiation they were measured directly, and when attenuated radiation was used the attenuation factor was estimated from the $SiH_3$ radical signal amplitude). [d] PDMS = poly(dimethylsiloxane), mean molecular mass = 100 000; $B_2O_3$ = boron oxide. [e] The rate constants in $cm^3$ $molecule^{-1}$ $s^{-1}$. The errors are one standard deviation of the linear regressions of the plots of $k'$ *vs* [NO] and represent the statistical scatter of the experimental points only. [f] From the global fit (see text). [g] The values in parentheses are obtained by the extrapolation of the low-temperature data.

**TABLE 2: Rate Constants for $SiD_3 + NO \rightarrow SiD_3NO$[a]**

| $T$/K[b] | [He]/$10^{16}$ [c] | $k_2/10^{-13}$ [d,e] |
|---|---|---|
| 302 | 3.83 | 13.1 ± 1.30 |
| 400 | 3.86 | 6.64 ± 0.45 |
| 400 | 7.85 | 9.41 ± 0.16 |
| 397 | 16.0 | 16.9 ± 0.53 |
| 505 | 0.80 | 1.26 ± 0.13 |
| 505 | 3.79 | 2.90 ± 0.08 |
| 506 | 7.77 | 4.52 ± 0.10 |
| 507 | 15.6 | 7.40 ± 0.29 |
| 605 | 3.81 | 1.49 ± 0.06 |
| 607 | 7.79 | 2.19 ± 0.06 |
| 611 | 15.6 | 3.54 ± 0.06 |
| From the Double-Exponential Kinetics [f] | | |
| 711 | 8.00 | 1.03 ± 0.28 (1.33)[g] |

[a] Experimental conditions: reactor, 1.05 cm i.d.; wall coating, $B_2O_3$; $SiD_3$ radical precursor, $SiD_3I$, [$SiD_3I$] = (1.0−1.5) × $10^{13}$ molecules $cm^{-3}$; wavelength, 248 nm; initial $SiD_3$ radical concentration, [$SiD_3$]$_0$ = (2.5−4.1) × $10^{10}$ molecules $cm^{-3}$ (estimated using the assumed quantum yield of $SiD_3$ radical from $SiD_3I$ equal to that of $SiH_3$ from $SiH_3I$ at 248 nm, 0.2 (ref 12), the precursor concentrations and the photodecomposition fractions). [b] Temperature uncertainty ±3 K. [c] Concentration in molecules $cm^{-3}$. [d] Rate constants in $cm^3$ $molecule^{-1}$ $s^{-1}$. [e] Errors are ±1 standard deviations and reflect statistical accuracy (scatter of points) only. [f] [$SiD_3I$] = 0.59 × $10^{13}$ molecules $cm^{-3}$, [$SiD_3$]$_0$ = 8.6 × $10^{10}$ molecules $cm^{-3}$. [g] The value in parentheses is obtained by the extrapolation of the low-temperature data.

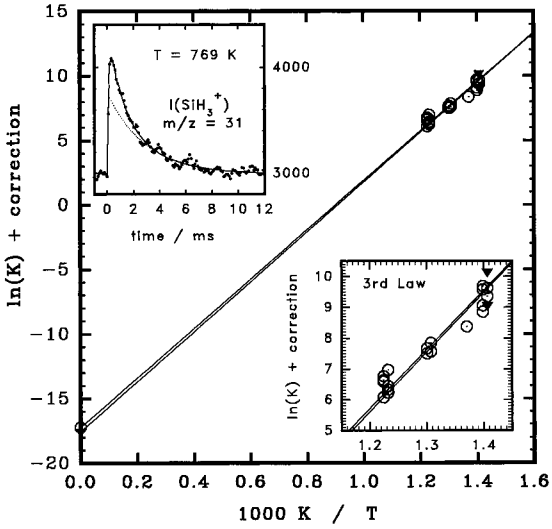


**Figure 3.** Modified van't Hoff plots of the equilibrium constants of the reactions $SiH_3 + NO \rightleftarrows SiH_3NO$ (circles) and $SiD_3 + NO \rightleftarrows SiD_3NO$ (triangles). The lines represent the third law fittings. The points at $1/T = 0$ used in the third law fit were calculated from thermodynamic functions of the reagents and product molecules ($SiH_3$, $SiD_3$, NO, $SiH_3$-NO, and $SiD_3NO$). Insert, top: an example of a double-exponential radical decay kinetics recorded at 769 K. Experimental conditions: [$SiH_3I$] = 7.05 × $10^{12}$ molecules $cm^{-3}$, $\lambda$ = 248 nm, [He] = 15.6 × $10^{16}$ molecules $cm^{-3}$, [NO] = 7.11 × $10^{15}$ molecules $cm^{-3}$, $T$ = 769 K, Cl lamp with $CaF_2$ window, $B_2O_3$ wall coating. The dotted line is the result of a single-exponential fit to the experimental points at $t$ > 4 ms. Insert, bottom: an enlarged portion of the main plot.

$P^\circ)^{-1}$ (standard state: ideal gas at $P^\circ$ = 1 bar). The standard enthalpy of reaction 1, $\Delta H^\circ_{298}$, was determined from the slope of the modified van't Hoff plot[26,27]

$$\ln(K) + \text{correction} = \Delta S^\circ_{298}/R - \Delta H^\circ_{298}/RT \quad (9)$$

$$\text{correction} = -\Delta(\delta S^\circ_{T,298})/R + \Delta(\delta H^\circ_{T,298})/RT \quad (10)$$

$$\delta S^\circ_{T,298} = S^\circ_T - S^\circ_{298}; \quad \delta H^\circ_{T,298} = H^\circ_T - H^\circ_{298} \quad (11)$$

where $\Delta S^\circ_{298}$ is the standard entropy of reaction 1.

The corrections for reactions 1 and 2 were calculated using the thermodynamic functions of $SiH_3NO$, $SiD_3NO$, $SiH_3$, $SiD_3$, and NO. Tabulated thermochemical data for NO were used.[28] The thermodynamic functions of $SiH_3NO$ and $SiH_3$ were calculated using the theoretical (*ab initio* + bond additivity corrections) structural parameters, vibrational frequencies, and, for the adduct molecules, the energy splittings between the two low-lying (singlet and triplet) electronic states (Melius and Allendorf[10]). The thermodynamic functions of $SiD_3NO$ and $SiD_3$ were calculated using the calculated sets of the vibrational frequencies and the moments of inertia for external and internal rotations. The vibrational frequencies were determined using the known frequencies for $SiH_3NO$ and $SiH_3$, the matrices of the normal mode vectors obtained in the *ab initio* calculations,[10] and the mass matrices. While more accurate thermodynamic functions of $SiH_3$, which account for anharmonicity of the inversion vibrational mode, are available,[29] the thermodynamic functions calculated in this work were used for the current thermochemical calculations for consistency.

The equilibrium constants for reactions 1 and 2 as well as the calculated corrections are given in Table 3. Two types of fits were used to obtain equilibrium constants from the experimental radical decay profiles—single profile fits and "global" fits. The two exponentials in the experimental double-

**TABLE 3: Equilibrium Constants for the Reactions $SiH_3$ + NO ⇄ $SiH_3NO$ and $SiD_3$ + NO ⇄ $SiD_3NO$**

| $T$/K[a] | [He]/$10^{16}$ [b] | [NO]/$10^{15}$ [b] | $k_w$/$s^{-1}$ [c] | ln($K$)[d] | ln($K$)[e] | correction [f] |
|---|---|---|---|---|---|---|
| | | | $SiH_3 + NO \rightleftarrows SiH_3NO$ | | | |
| 711 | 8.77 | 1.35[g] | 182 | 9.51 | 9.07 ± 0.81[h] | −0.16 |
| | | 2.02[g] | | 9.78 | | |
| 715 | 15.66 | 0.95 | 179 | 9.01 | 8.58 ± 0.14 | −0.16 |
| | | 1.03 | | | | |
| | | 2.23 | | 9.72 | | |
| | | 3.86 | | 9.84 | | |
| | | 5.52 | | | | |
| | | 5.76 | | 9.74 | | |
| | | 6.64 | | | | |
| 730 | 30.68 | 1.98[g] | 300 | 8.53 | 8.53 ± 0.12 | −0.18 |
| 765 | 8.73 | 2.41[g] | 207 | 8.04 | 7.98 ± 0.25 | −0.20 |
| | | 4.93[g] | | 7.76 | | |
| 769 | 15.60 | 3.17 | 178 | 7.70 | 8.02 ± 0.39 | −0.21 |
| | | 7.11 | | 7.87 | | |
| 812 | 3.78 | 1.93 | 180 | | 6.47 ± 0.23 | −0.24 |
| | | 3.54 | | | | |
| | | 5.15 | | 7.21 | | |
| | | 6.35 | | 6.46 | | |
| | | 6.62 | | 6.68 | | |
| | | 8.64 | | 6.57 | | |
| 817 | 15.59 | 1.08 | 207 | | 7.18 ± 0.25 | −0.25 |
| | | 1.86 | | 6.32 | | |
| | | 4.17 | | 6.83 | | |
| | | 7.01 | | 7.01 | | |
| | | 8.70 | | 6.85 | | |
| | | 9.38 | | 6.88 | | |
| | | 10.38 | | | | |
| | | | $SiD_3 + NO \rightleftarrows SiD_3NO$ | | | |
| 711 | 8.00 | 1.94 | 446 | 9.30 | | −0.24 |
| 711 | 8.00 | 5.67 | 446 | 10.38 | | −0.24 |

[a] Temperature uncertainty ±3 K. [b] Concentration in molecules $cm^{-3}$. [c] The rate constant of wall decay ($k_4$ for $SiH_3$ radical, $k_5$ for $SiD_3$ radical). [d] The equilibrium constant obtained by fitting of individual kinetics by a double-exponential function. $K = (P_{SiH_3NO}/P^\circ)(P_{SiH_3}/P^\circ)^{-1}(P_{NO}/P^\circ)^{-1}$ is dimensionless thermodynamic equilibrium constant (standard state, ideal gas at $P^\circ = 1$ bar). [e] The equilibrium constant obtained by a global fitting of all experimental profiles at the same temperature (see text for details). [f] See text for definition. [g] Poly(dimethylsiloxane) (PDMS) wall coating, in all other experiments $B_2O_3$ was used. [h] The error is one standard deviation of the fit and reflects statistical accuracy only.

exponential profiles are not well separated in the current experiments due to the following reasons. First, the reactions under study (1 or 2) are essentially in the pressure falloff region at the experimental conditions used, and large concentrations of NO are required to provide a reaction rate comparable to the rate of radical decay on the reactor wall. At these high concentrations of NO, reaction 3 (and its deuterium-substituted analog) contributes significantly to the radical decay kinetics. Second, the isotope peak of NO ($^{15}N^{16}O^+$) overlaps with the parent ion of $SiH_3$ at $m/z = 31$ and gives a considerable contribution to the "base line" signal, which reduces the signal/noise ratio of the ion signal temporal profiles. Only a limited number of the experimental profiles allowed separation of the two exponentials. To improve the reliability of the extracted parameters, a global fit of a set of kinetic profiles obtained at the same experimental conditions with variable concentration of NO added was attempted. The procedure is illustrated on the set of kinetic profiles recorded at 715 K (Table 3). Seven kinetic profiles were recorded with NO added and two without NO (to determine the wall decay constant). Only four of the seven profiles were suitable for the double-exponential fitting. In each case four *independent* fitting parameters were used ($A_1$, $A_2$, $\lambda_1$, and $\lambda_2$ for each temporal profile); therefore, the total number of the fitting parameters was 16, with experimental information from four profiles. In the *global* fit, all seven experimental profiles were fitted to the fitting function that contains only 11 fitting parameters (seven initial amplitudes, $k_1$, $k_{-1}$, $k_3$, and $k_6$). Due to the *reduction* in the number of the fitting parameters as well as utilization of *additional* experimental information from the three extra profiles (which is discarded in the usual approach), the standard deviation of the global fit was improved compared to the single profile fits. The equilibrium data obtained using the global fitting procedure together with the results of the single profile fits are given in the Table 3. It should be noted, however, that, in spite of a significant improvement in the standard deviation of the resulting equilibrium constants at individual temperatures, the quality (scatter of points) of the modified van't Hoff plot was not improved by the global fit procedure.

The rate constants of reactions 1−3 obtained in the fits of the double-exponential kinetics are listed in Tables 1−3. In the most reliable cases rate constants agree with the values obtained by the extrapolation of the low-temperature data within 20−30%. Rate constants of reaction 3 obtained in the fittings, as shown in Figure 6, are in good agreement with extrapolation from low-temperature measurements.

Modified van't Hoff plots of the equilibrium constants of reactions 1 and 2 are shown in Figure 3. The lines drawn through the experimental points in Figure 3 are the third law fits using the calculated standard entropy of the reactions 1 and 2:

$$\Delta S^\circ_{298}(\text{rxn 1}) = -143.1 \text{ J mol}^{-1} \text{ K}^{-1} \quad \text{(calculated)} \quad (12)$$

$$\Delta S^\circ_{298}(\text{rxn 2}) = -146.0 \text{ J mol}^{-1} \text{ K}^{-1} \quad \text{(calculated)} \quad (13)$$

The third law procedure uses these calculated reaction entropies as the ordinate intercepts of the modified van't Hoff plots (intercept = $\Delta S^\circ_{298}/R$) and provides the following standard enthalpies of reactions 1 and 2 from the slopes of the lines through the corrected equilibrium constants and the intercepts:

$$\Delta H^\circ_{298}(\text{rxn 1}) = -158.9 \pm 5.7 \text{ kJ mol}^{-1} \quad \text{(third law procedure)} \quad (14)$$

$$\Delta H^\circ_{298}(\text{rxn 2}) = -160.5 \pm 7.3 \text{ kJ mol}^{-1} \quad \text{(third law procedure)} \quad (15)$$

The errors are one standard deviations of the fits plus the errors due to the accuracy of the gas flow, pressure measurements, and the temperature uncertainty.

The accuracies of $\Delta H^\circ_{298}$ of reactions 1 and 2 determined by the third law method were estimated as follows. The accuracy of the equilibrium constants measured in the middle part of the temperature range studied (711−817 K) is determined by their statistical scatter, by the errors of the gas flow measurements, and by the temperature uncertainty. The standard deviations of the fits due to the scatter of experimental points are ±2.3 and ±3.9 kJ $mol^{-1}$ for reactions 1 and 2, respectively. The combined error introduced into $K_p$ by the small uncertainties of pressure and flow measurements and the temperature uncertainty (±3 K) is estimated as 22%, leading to the errors in the standard enthalpies of the reactions ±1.4 kJ $mol^{-1}$.

The intercept of the modified van't Hoff plot is obtained from the calculated standard entropy of reaction 1. In general, theoretical calculations provide reliable structural parameters, and the accuracy of the calculated thermodynamic functions depends mainly on the accuracy of calculated vibrational

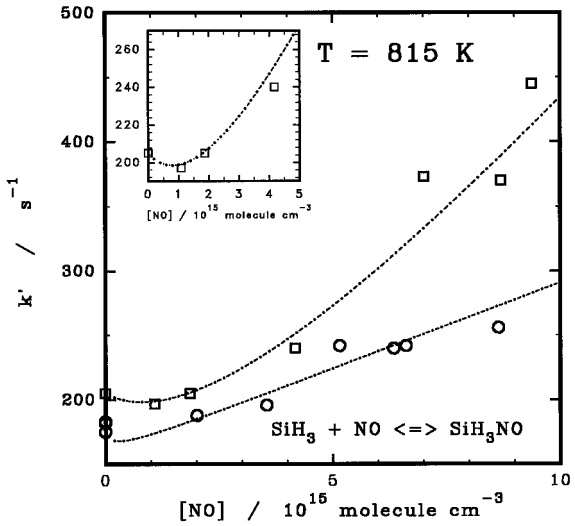


**Figure 4.** Parameter of the long-lived exponential ($\lambda_2$) of $SiH_3$ radical measured as a function of NO concentration at 815 K at two different buffer gas densities ([He] = $3.78 \times 10^{16}$ molecules $cm^{-3}$ for the lower curve and $15.6 \times 10^{16}$ molecules $cm^{-3}$ for the upper curve). The dashed line show the fitting results (see text). Insert: enlarged portion of the upper curve at low concentrations of NO.

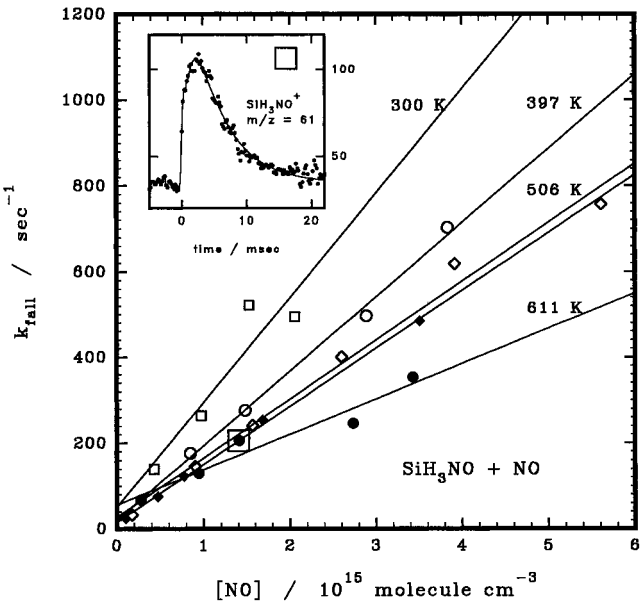


**Figure 5.** Pseudo-first-order rate constant of reaction $SiH_3NO + NO \rightarrow$ products vs NO concentration at different temperatures. Insert: an example of the $SiH_3NO$ rise and decay kinetics. The experimental point corresponding to the displayed kinetics is indicated by the square. Experimental conditions: $[SiH_3I] = 1.94 \times 10^{12}$ molecules $cm^{-3}$, $\lambda =$ 248 nm, $[He] = 15.7 \times 10^{16}$ molecules $cm^{-3}$, $[NO] = 1.44 \times 10^{15}$ molecules $cm^{-3}$, $T = 611$ K, H lamp with $MgF_2$ window, $B_2O_3$ wall coating.

frequencies, especially of the low-frequency torsional modes. An empirical correction (*ca.* −11%) was applied to the calculated frequencies. The simultaneous change of all frequencies (including torsional) of $SiH_3$ radical and $SiH_3NO$ molecule by one-half of this correction (±6%) leads to a change of the standard enthalpy of reaction 1, as determined by the third-law procedure, of ±1.0 kJ $mol^{-1}$. The torsional potential barrier (*ca.* 1.9 kJ $mol^{-1}$) in our calculations was obtained from the torsional frequency assuming 3-fold sinusoidal potential. The *ab initio* value is somewhat different, *ca.* 4 kJ $mol^{-1}$.[15] Change of the torsional barrier from 1.9 to 4 kJ $mol^{-1}$ leads to the standard enthalpy change of 0.6 kJ $mol^{-1}$. A possible error of ±0.4 kJ $mol^{-1}$ was estimated due to an uncertainty in the singlet−triplet splitting in $SiH_3NO$. The final estimate of the accuracy of the third-law determinations (±5.7 kJ $mol^{-1}$ for reaction 1) was obtained by summing all errors considered above.

The second-law procedure which utilizes only the slope of the data in the modified van't Hoff plot was not used due to the scatter of experimental points (Figure 3).

Additional proofs on the existence of equilibrium in reaction 1 at temperatures 611−817 K were obtained by observing the dependence of the long-lived exponential's lifetime on the concentration of NO at high temperatures. Figure 4 shows the dependencies of $\lambda_2$ (the decay parameter of the long-lived exponential) on the concentration of NO at two different buffer gas densities (He) at 815 K. An interesting feature of these dependencies is the initial decrease of $\lambda_2$ with the concentration at low NO concentrations. The decay parameters of the short-lived and long-lived exponentials are determined by expression 16:[19,20]

$$\lambda_{1,2} = (k_4 + k'_1 + k_{-1} + k'_3)/2 \pm \{((k_4 + k'_1 - k_{-1} - k'_3)/2)^2 + k'_1 k_{-1}\}^{1/2} \quad (16)$$

The pseudo-first-order rate constants were previously defined. The minus sign corresponds to the decay parameter of the long-lived exponential, $\lambda_2$. This expression predicts an initial decrease of $\lambda_2$ (increase of $SiH_3$ lifetime at long times) with NO concentration, due to the lower rate of consumption of $SiH_3$, when it is bound in $SiH_3NO$ compared to the rate of wall recombination of free $SiH_3$ radical. This behavior is observed experimentally and is well reproduced by simulation of $\lambda_2$ using expression 16. The dashed lines in Figure 4 represent the results of a simultaneous fit of both curves using the mechanism which consists of reactions 1, −1, 3, and 6. The extrapolated value of the ratio of the rate constants of reaction 1 at these two different buffer gas densities (3.41 at 815 K) was used as a fixed parameter. The bond energy, the rate constant of reaction 1, and the rate constant of reaction 3 were used as the fitting parameters. The value of the bond energy obtained using this procedure, $DH°_0(H_3Si-NO) = 153.2$ kJ $mol^{-1}$, is in excellent agreement with the value obtained from the equilibrium constant measurements. The values of $k_1$ and $k_3$ at 815 K obtained in the fit are in good agreement with those obtained by extrapolation of the low-temperature data.

**Kinetics of the Reaction $SiH_3NO + NO \rightarrow$ Products.** The adduct ($SiH_3NO$) formation and decay caused by reactions 1, 3, and 6 were also recorded and studied. A typical $SiH_3NO$ signal is shown in Figure 5 (insert). The rise and decay times are well-separated, and measuring the dependence of the decay time on the concentration of NO added permits the determination of the rate constant of reaction 3. The rate constants determined from the rise times are in good agreement with those obtained in the $SiH_3$ radical decay kinetic measurements. This fact allows an unambiguous assignment of the decay time of $SiH_3NO$ kinetic profiles to reactions 3 and 6. Plots of the pseudo-first-order rate constants *vs* [NO] are shown in Figure 5. The rate constants of reaction 3, determined from the slopes of the straight lines drawn through the data as shown in Figure 5, are given in Table 4. The rate constants obtained by the global fits of the double-exponential kinetics are also shown for comparison. The rate constant has a negative temperature dependence (Figure 6). In the temperature range studied (301−611 K) the temperature dependence is

**TABLE 4: Rate Constants for $SiH_3NO + NO \rightarrow$ Products[a]**

| $T$/K[b] | [He]/$10^{16}$ [c] | $k_3/10^{-13}$ [d,e] |
|---|---|---|
| 303 | 16.0 | $2.92 \pm 0.68$ |
| 397 | 16.1 | $1.62 \pm 0.11$ |
| 505 | 3.81 | $1.44 \pm 0.15$ |
| 507 | 15.8 | $1.45 \pm 0.08$ |
| 611 | 15.7 | $0.82 \pm 0.12$ |
| From the Double-Exponential Kinetics | | |
| 711 | 8.77 | $0.55 \pm 0.35$ |
| 715 | 15.7 | $1.38 \pm 0.46$ |
| 730 | 30.7 | $0.45 \pm 0.09$ |
| 765 | 8.73 | $0.81 \pm 0.17$ |
| 769 | 15.6 | $1.00 \pm 0.30$ |
| 812 | 3.78 | $0.74 \pm 0.14$ |
| 817 | 15.6 | $0.69 \pm 0.13$ |

[a] Experimental conditions: reactor, 1.05 cm i.d.; wall coating, $B_2O_3$; $SiH_3$ radical precursor, $SiH_3I$, $[SiH_3I] = (1.8-2.56) \times 10^{12}$ molecules $cm^{-3}$; wavelength, 248 nm; the precursor photodecomposition fraction, 1.1−2.2%; initial $SiH_3$ radical concentration, $[SiH_3]_0 = (0.4-1.1) \times 10^{10}$ molecules $cm^{-3}$ (estimated using the quantum yield of $SiH_3$ radical from $SiH_3I$ at 248 nm, 0.2 (ref 12), the precursor concentrations, and the photodecomposition fractions). [b] Temperature uncertainty ±3 K. [c] Concentration in molecules $cm^{-3}$. [d] Rate constants in $cm^3$ $molecule^{-1}$ $s^{-1}$. [e] Errors are ±1 standard deviations and reflect statistical accuracy (scatter of points) only.

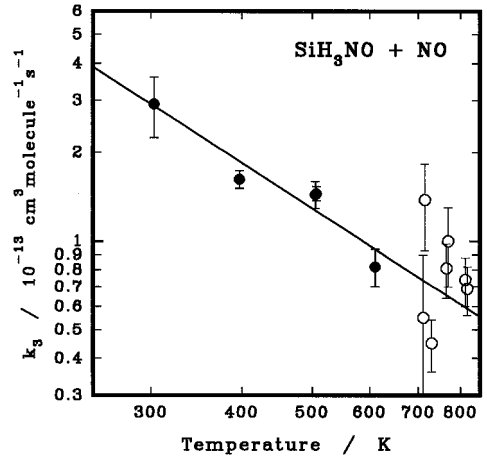


**Figure 6.** Temperature dependence of the rate constant of $SiH_3NO$ + NO reaction in log−log coordinates. Solid circles: direct measurements at 300−611 K. Only these points were used for regression (solid line). Open circles: extracted from the double-exponential kinetics.

$$k_3 = (2.95 \pm 0.38) \times 10^{-13}(T/298)^{-1.59\pm0.29} \text{ cm}^3 \text{ molecule}^{-1} \text{ s}^{-1} \quad (17)$$

No buffer gas density dependence of the rate constant of reaction 3 was found at 505 K by varying the He density by a factor of 4.1 (Table 4).

### RRKM Analysis of Reactions 1 and 2

Simple estimates show that reactions 1 and 2 are nessesarily in the pressure falloff regions if the limiting high-pressure rate constants do not differ significantly from those typical for association reactions of free radicals with oxygen and nitric oxide.[10,30−37] Assuming that the high-pressure rate constant of reaction 1 is *ca.* $(1-3) \times 10^{-11}$ $cm^3$ $molecule^{-1}$ $s^{-1}$,[10,30−37] and the value reported by Sugawara *et al.*[11] ($8.2 \times 10^{-30}$ $cm^6$ $molecule^{-2}$ $s^{-1}$, 300 K) is the true low-pressure limit value, for the buffer gas density of $32 \times 10^{16}$ molecules $cm^{-3}$ one obtains $k_0 = 2.6 \times 10^{-12}$ $cm^3$ $molecule^{-1}$ $s^{-1}$. Therefore, the dimensionless parameter $x = k_0/k_{inf}$ is estimated as 0.26 −0.086. Simple falloff estimates show that deviations from the true low-pressure limit of a factor of *ca.* 2−3 can be expected at these values of $k_0/k_{inf}$. In turn, it means that the true low-pressure limit rate constant is factor of 2−3 higher. Then the $x$ values are 2−3 times higher, and even larger deviations are anticipated.

The Troe factorization approach was used to calculate the low-pressure limit[38] and pressure falloff curves[39] for $k_1$ and $k_2$. Both the ground singlet state and the low-lying excited triplet electronic state of $SiH_3NO$[10] were taken into account. The importance of bound triplet states for dissociation−recombination reactions has been discussed by Smith[32] and Davies *et al.*[30] The two limiting cases when the unknown rate of collision-induced and collisionless transitions between the states is not required for the falloff calculations were discussed in our previous paper on $Si(CH_3)_3 + NO$ recombination reaction.[10] In the first limiting case, the rate of collisionless and collision-induced transition between the electronic states is much smaller than the rate of collisional deactivation within the electronic states. Here the electronic states may be treated separately. In the second limiting case (interstate mixing is much faster than collisional relaxation within the states), the joint manifold of the rovibrational states can be used in the RRKM calculations. Since the rate of singlet−triplet transitions in the $SiH_3NO$ molecule is unknown, and the collisional relaxation of highly vibrationally excited molecules is fast, the first model was used in the falloff calculations. Both electronic states are considered to contribute independently to the recombination rate, with the two contributions having separate buffer gas pressure falloff dependencies.

The rate constant of recombination reaction 1 (or 2) is represented as

$$k_{rec} = k^{S}_{rec,inf}(x_1/(1+x_1))F_1(x_1) + k^{T}_{rec,inf}(x_2/(1+x_2))F_2(x_2) \quad (18)$$

where $k^{S}_{rec,inf}$ and $k^{T}_{rec,inf}$ are the high-pressure limit recombination constants into the singlet and triplet states, $F_1(x_1)$ and $F_2(x_2)$ are the broadening pressure falloff factors for the singlet and triplet states, and $x_1$ and $x_2$ are the dimensionless buffer gas density parameters:

$$x_1 = \beta_c k_{tri}^{S,sc}[M]/k^{S}_{rec,inf} \qquad x_2 = \beta_c k_{tri}^{T,sc}[M]/k^{T}_{rec,inf} \quad (19)$$

In these expressions, $\beta_c$ is the weak collision efficiency, $k_{tri}^{S,sc}$ and $k_{tri}^{T,sc}$ are the low-pressure limit strong collision third-order recombination rate constants into the singlet and triplet states, and [M] is the buffer gas density.

In the calculations below two general assumptions have been made: the collision efficiencies for the triplet and singlet states are assumed to be equal, and the high-pressure recombination rate into the triplet state is assumed to be 3 times larger than the rate constant of recombination into the singlet state:

$$k^{T}_{rec,inf} = 3k^{S}_{rec,inf} \quad (20)$$

The latter assumption is equivalent to the assumption of the same structure and properties of the "transition states" for the recombination into the triplet and singlet states and reflects the statistical weights of these states.

In the falloff calculations the total high-pressure recombination rate constant, $k_{rec,inf}$, and the weak collision efficiency, $\beta_c$, served as fitting parameters. The low-pressure limit rate constants were calculated based on the structures, vibrational frequencies, and the triplet−singlet splitting provided by the *ab initio*−BAC calculations.[10] The strong collision rate constant of recombination in the low-pressure limit is expressed as[38]

**TABLE 5: Calculated Thermodynamic Functions of $SiH_3NO$ (Standard State 1 bar ≡ $10^5$ Pa)**

| $T$, K | $S°$, J mol$^{-1}$ K$^{-1}$ | $H°_T - H°_0$, kJ mol$^{-1}$ | $C_p°$, J mol$^{-1}$ K$^{-1}$ |
|---|---|---|---|
| 150 | 246.73 | 6.0556 | 46.075 |
| 200 | 260.77 | 8.5035 | 52.311 |
| 250 | 273.26 | 11.308 | 59.907 |
| 298.15 | 284.47 | 14.374 | 67.463 |
| 300 | 284.89 | 14.499 | 67.747 |
| 350 | 295.89 | 18.070 | 75.021 |
| 400 | 306.33 | 21.989 | 81.353 |
| 450 | 316.23 | 26.198 | 86.681 |
| 500 | 325.60 | 30.648 | 91.096 |
| 550 | 334.46 | 35.299 | 94.763 |
| 600 | 342.84 | 40.119 | 97.856 |
| 650 | 350.78 | 45.082 | 100.50 |
| 700 | 358.31 | 50.166 | 102.79 |
| 750 | 365.47 | 55.357 | 104.80 |
| 800 | 372.29 | 60.640 | 106.59 |
| 850 | 378.80 | 66.008 | 108.19 |
| 900 | 385.03 | 71.451 | 109.64 |
| 950 | 390.99 | 76.963 | 110.94 |
| 1000 | 396.71 | 82.538 | 112.13 |
| 1100 | 407.50 | 93.854 | 114.20 |
| 1200 | 417.51 | 105.37 | 115.93 |
| 1300 | 426.86 | 117.05 | 117.40 |
| 1400 | 435.61 | 128.86 | 118.64 |
| 1500 | 443.83 | 140.79 | 119.70 |
| 1600 | 451.59 | 152.81 | 120.63 |
| 1700 | 458.92 | 164.93 | 121.42 |
| 1800 | 465.88 | 177.11 | 122.11 |
| 1900 | 472.50 | 189.36 | 122.72 |
| 2000 | 478.81 | 201.67 | 123.25 |

[a] $SiH_3NO$ molecular parameters: Molecular mass 60.998. $SiH_3NO$, singlet state (cis): frequencies (cm$^{-1}$, see footnote *b*): 307, 563, 585, 711, 908, 919, 923, 1705, 2158, 2165, 2171; main moments of inertia (see footnote *c*) $1.928 \times 10^{-46}$, $1.396 \times 10^{-45}$, $1.490 \times 10^{-45}$ kg m$^2$; symmetry number for external rotation, $\sigma_{ext} = 1$; one hindered rotor with the reduced moment of inertia (see footnote *c*) $5.307 \times 10^{-47}$ kg m$^2$ and barrier for internal rotation 1.90 kJ mol$^{-1}$, respectively (see footnote *d*); symmetry number for internal rotor, $\sigma_{introt} = 3$; electronic degeneracy = 1. $SiH_3NO$, triplet state (trans): frequencies (cm$^{-1}$, see footnote *b*): 214, 624, 638, 686, 926, 928, 935, 1674, 2162, 2163, 2187; main moments of inertia (see footnote *c*) $1.605 \times 10^{-46}$, $1.479 \times 10^{-45}$, and $1.542 \times 10^{-45}$ kg m$^2$; symmetry number for external rotations, $\sigma_{ext} = 1$; one hindered rotor with the reduced moment of inertia (see footnote *c*) $4.269 \times 10^{-47}$ kg m$^2$ and barrier for internal rotation (see footnote *d*) 2.46 kJ mol$^{-1}$, respectively; symmetry numbers for internal rotor, $\sigma_{introt} = 3$; electronic degeneracy = 3. Triplet−singlet splitting = 12.54 kJ mol$^{-1}$. [b] Frequencies calculated at the HF/6-31G* level and scaled (scaling factor 0.893).[10] [c] Moments of inertia of external and internal rotation calculated using molecular structure optimized at the same level of theory. Reduced moments of inertia calculated according to Pitzer and Gwinn.[46] [d] Barriers calculated from torsional frequencies and assumed three-cycle sinusoidal potential for internal rotations. Contributions to thermodynamic functions for hindered rotors obtained by linear interpolation of tables.[46]

**TABLE 6: Calculated Thermodynamic Functions of $SiD_3NO$ (Standard State 1 bar ≡ $10^5$ Pa)[a]**

| $T$, K | $S°$, J mol$^{-1}$ K$^{-1}$ | $H°_T - H°_0$, kJ mol$^{-1}$ | $C_p°$, J mol$^{-1}$ K$^{-1}$ |
|---|---|---|---|
| 150 | 252.19 | 6.2180 | 49.800 |
| 200 | 267.73 | 8.9278 | 58.656 |
| 250 | 281.82 | 12.091 | 67.886 |
| 298.15 | 294.50 | 15.562 | 76.271 |
| 300 | 294.97 | 15.704 | 76.577 |
| 350 | 307.38 | 19.736 | 84.345 |
| 400 | 319.08 | 24.128 | 90.980 |
| 450 | 330.13 | 28.821 | 96.477 |
| 500 | 340.53 | 33.764 | 100.97 |
| 550 | 350.33 | 38.908 | 104.60 |
| 600 | 359.56 | 44.215 | 107.56 |
| 650 | 368.27 | 49.653 | 109.97 |
| 700 | 376.49 | 55.202 | 111.98 |
| 750 | 384.27 | 60.841 | 113.65 |
| 800 | 391.65 | 66.556 | 115.08 |
| 850 | 398.67 | 72.338 | 116.29 |
| 900 | 405.34 | 78.177 | 117.35 |
| 950 | 411.71 | 84.068 | 118.27 |
| 1000 | 417.80 | 90.009 | 119.08 |
| 1100 | 429.23 | 102.00 | 120.45 |
| 1200 | 439.76 | 114.11 | 121.54 |
| 1300 | 449.53 | 126.32 | 122.43 |
| 1400 | 458.63 | 138.61 | 123.18 |
| 1500 | 467.15 | 150.96 | 123.80 |
| 1600 | 475.16 | 163.38 | 124.33 |
| 1700 | 482.71 | 175.84 | 124.79 |
| 1800 | 489.85 | 188.35 | 125.18 |
| 1900 | 496.63 | 200.89 | 125.52 |
| 2000 | 503.07 | 213.46 | 125.82 |

[a] $SiD_3NO$ molecular parameters: Molecular mass 64.017. $SiD_3NO$, singlet state (cis): frequencies (cm$^{-1}$, see footnote *b*): 277, 444, 482, 617, 663, 667, 712, 1534, 1563, 1567, 1706; main moments of inertia (see footnote *c*) $2.894 \times 10^{-46}$, $1.552 \times 10^{-45}$, $1.645 \times 10^{-45}$ kg m$^2$; symmetry number for external rotation, $\sigma_{ext} = 1$; one hindered rotor with the reduced moment of inertia (see footnote *c*) $6.197 \times 10^{-47}$ kg m$^2$ and barrier for internal rotation 1.57 kJ mol$^{-1}$, respectively (see footnote *d*); symmetry number for internal rotor, $\sigma_{introt} = 3$; electronic degeneracy = 1. $SiD_3NO$, triplet state (trans): frequencies (cm$^{-1}$, see footnote *b*): 204, 483, 514, 615, 669, 674, 699, 1540, 1562, 1584, 1674; main moments of inertia (see footnote *c*) $2.571 \times 10^{-46}$, $1.639 \times 10^{-45}$, and $1.701 \times 10^{-45}$ kg m$^2$; symmetry number for external rotations, $\sigma_{ext} = 1$; one hindered rotor with the reduced moment of inertia (see footnote *c*) $5.724 \times 10^{-47}$ kg m$^2$ and barrier for internal rotation (see footnote *d*) 2.48 kJ mol$^{-1}$, respectively; symmetry numbers for internal rotor, $\sigma_{introt} = 3$; electronic degeneracy = 3. Triplet−singlet splitting = 12.31 kJ mol$^{-1}$. [b] Frequencies calculated at the HF/6-31G* level and scaled (scaling factor 0.893).[10] [c] Moments of inertia of external and internal rotation calculated using molecular structure optimized at the same level of theory. Reduced moments of inertia calculated according to Pitzer and Gwinn.[46] [d] Barriers calculated from torsional frequencies and assumed three-cycle sinusoidal potential for internal rotations. Contributions to thermodynamic functions for hindered rotors obtained by linear interpolation of tables[46]

$$k_{tri}^{sc} = Z_{LJ}(\rho_{vib,h}(E_0)kT/Q_{vib,h})F_E F_{anh} F_{rot} F_{introthind} \times (Q_{SiH_3NO}/Q_{SiH_3} Q_{NO}) \quad (21)$$

with the usual meaning of the symbols. $Z_{LJ}$ is the Lennard-Jones collision number, $\rho_{vib,h}(E_0)$ is the vibrational density of states of the $SiH_3NO$ molecule at the threshold energy for dissociation, $E_0$, in the harmonic oscillator approximation, and $Q_{vib,h}$ is the vibrational partition function of the $SiH_3NO$ molecule in the harmonic approximation. $F_E$, $F_{anh}$, $F_{extrot}$, and $F_{introthind}$ are correction factors accounting for the energy dependence of the vibrational density of states, for the effect of the anharmonicity of vibrations, and for the influence of the centrifugal barrier and for hindered internal rotors. In calculating these parameters, the torsional motion of the molecule was treated as a free internal rotor. Corrections for hindrance were made in $F_{introthind}$.[38] The experimentally determined "well depth", $E_0$, for the singlet state was used ($E_0$(singlet) = $-\Delta H°_0$, assuming the absence of an additional barrier). For the triplet state, the singlet state value minus the theoretically calculated triplet−singlet splitting[10] was used. The scaled vibrational frequencies, molecular structures, moments of inertia for external and internal rotations, and triplet−singlet splitting were obtained from the theoretical (*ab initio* + BAC) calculations.[10] The barriers for the hindered rotors were determined from the scaled calculated torsional frequencies and reduced moments of inertia assuming a three-cycle sinusoidal potential for the internal rotations. The Lennard-Jones collision number[40] was calculated using the parameters $\sigma$(He) = 2.55 Å, $\epsilon$(He) = 10 K, $\sigma$($SiH_3$-NO) = 4.69 Å, and $\epsilon$($SiH_3NO$) = 294 K. The collision diameter of $SiH_3NO$ was estimated using the relationship $\sigma = 1.18V_b^{1/3}$,[41] $V_b$ estimated as a sum of Le Bas atomic increments ($V_C$ = 14.8,

**TABLE 7: Coefficients of NASA Polynomials[a,b] for NO, $SiH_3$, $SiD_3$, $SiH_3NO$ (Singlet), $SiH_3NO$ (Triplet), $SiH_3NO$, $SiD_3NO$ (Singlet), $SiD_3NO$ (Triplet), and $SiD_3NO$**

| molecule | $a_1$ | $a_2 \times 10^3$ | $a_3 \times 10^6$ | $a_4 \times 10^9$ | $a_5 \times 10^{12}$ | $a_6$ | $a_7$ |
|---|---|---|---|---|---|---|---|
| NO[c] | 4.2287 | −4.7511[c] | 11.376 | −9.7243 | 2.9582 | −26.771 | 2.2459 |
| $SiH_3$[d] | 2.8526 | 7.3944 | −1.4390 | −1.1159 | 0.40400 | 90.311 | 7.6980 |
| $SiD_3$[e] | 2.3846 | 13.493 | −10.007 | 3.41640 | −0.43716 | 107.27 | 10.431 |
| $SiH_3NO$ [f] (singlet) | 2.5614 | 21.365 | −16.144 | 6.0613 | −0.90821 | 121.43 | 13.811 |
| $SiH_3NO$ [f] (triplet) | 2.6750 | 20.756 | −15.231 | 5.5230 | −0.79829 | 133.16 | 14.452 |
| $SiH_3NO$ [f] | 0.83770 | 33.322 | −33.817 | 16.032 | −2.8585 | 272.11 | 20.891 |
| $SiD_3NO$[g] (singlet) | 2.5266 | 26.827 | −24.425 | 10.605 | −1.7731 | 92.957 | 13.906 |
| $SiD_3NO$[g] (triplet) | 2.8588 | 25.444 | −22.444 | 9.4432 | −1.5345 | 74.830 | 13.536 |
| $SiD_3NO$[g] | 1.0885 | 37.697 | −40.510 | 19.605 | −3.5156 | 201.16 | 19.641 |

[a] Polynomial representation of thermodynamic functions:[45] $C°_P(T)/R = a_1 + a_2T + a_3T^2 + a_4T^3 + a_5T^4$; $(H°(T) - H°(0))/RT = a_1 + a_2T/2 + a_3T^2/3 + a_4T^3/4 + a_5T^4/5 + a_6/T$; $S°(T)/R = a_1 \ln(T) + a_2T + a_3T^2/2 + a_4T^3/3 + a_5T^4/4 + a_7$. [b] Temperature range 250−2000 K, except for NO. [c] Temperature range 250−1000 K, data from ref 28 were used for fitting. [d] $SiH_3$ parameters: mass 31.000; frequencies ($cm^{-1}$): 781, 906(2), 2111, 2128(2); main moments of inertia $5.889 \times 10^{-47}$, $5.889 \times 10^{-47}$, $9.889 \times 10^{-47}$ kg $m^2$; $\sigma_{ext} = 3$; $g_{el} = 2$. [e] $SiD_3$ parameters: mass 34.019; frequencies ($cm^{-1}$): 577, 654(2); 1501, 1537(2); main moments of inertia $1.160 \times 10^{-46}$, $1.160 \times 10^{-46}$, and $1.976 \times 10^{-46}$ kg $m^2$; $\sigma_{ext} = 3$; $g_{el} = 2$. [f] See footnotes to Table 5. [g] See footnotes to Table 6.

$V_H = 3.7$, $V_O = 7.4$, $V_N = 10.5$, all from ref 41, and $V_{Si} = 33.7$[42]). The Lennard-Jones potential well depth for $SiH_3$ was estimated using the relationships $\epsilon/K = 1.21T_b$; $T_b(SiH_3NO) \cong$ 243 K as it is for $SiH_3Cl$.

The calculated $Z_{LJ}$ for $298 \le T \le 1000$ K is

$$Z_{LJ}(SiH_3NO-He) = 4.83 \times 10^{-10}(T/298)^{0.35} \quad (22)$$

The rate constants of recombination into the triplet and singlet states are given by expression 21 with the parameters densities of states and the partition functions corresponding to the triplet and singlet states and with the threshold energies $E_0$(singlet)= $E_0 = -\Delta H°_0$ and $E_0$(triplet) = $E_0 - \Delta E_{T-S}$, $\Delta E_{T-S}$ being the triplet−singlet splitting.

Standard expressions were used to calculate the general broadening factors $F_1(x_1)$, $F_2(x_2)$[43] and $F_{cent,1}$, $F_{cent,2}$[39] that enter expression 18. Since the calculations showed that the parameters $F_{cent}$ differ by less than 2% for the singlet and triplet states over the range 301−611 K, a single $F_{cent}$ parameter (average) was used in the falloff calculations. Finally, eq 18 was used to fit the experimental data in the temperature range 301−611 K using $\beta_c$ and the total high-pressure rate constant as fitting parameters. The weak collision efficiency was assumed to be independent of temperature. Parameter *n*, the parameter of the temperature dependence of the high-pressure recombination rate constant, expression 23, was fixed at $n = -1$.

$$k_{rec,inf} = k_{rec,inf,298}(T/298)^n \quad (23)$$

Two separate fits have been performed for reactions 1 and 2. All temperature dependencies were fitted simultaneously. The fit of the falloff data for reaction 1 using $E_0 = 153.7$ kJ $mol^{-1}$ yielded the weak collision efficiency factor $\beta_c = 0.153$ and the high-pressure limit rate constany of reaction 1, $k_{1,inf} = (3.9 \pm 1.1) \times 10^{-11}$ $cm^3$ $molecule^{-1}$ $s^{-1}$. The fit of the data for reaction 2 using $E_0 = 153.7 + 2.4 = 156.1$ kJ $mol^{-1}$ (2.4 kJ $mol^{-1}$ is calculated using the difference in zero-point vibrational energies for reactions 1 and 2) resulted in the weak collision efficiency $\beta_c = 0.146$ and the high-pressure limit rate constant of reaction 2, $k_{2,inf} = (5.0 \pm 1.3) \times 10^{-11}$ $cm^3$ $molecule^{-1}$ $s^{-1}$. There is a very good agreement between the weak collision efficiencies produced by the fits of the sets of data for reactions 1 and 2. The absolute value of $\beta_c$ as well as the high-pressure limit rate constants is quite typical for this type of reaction.[10,30−37,44]

The pressure falloff curves fitted to the experimental points using the procedure described above are shown by solid lines in Figure 2. The parametrizations of the rate constants of reactions 1 and 2 are the following (301−611 K).

$$k_{1,tri} = (3.12 \pm 0.12) \times 10^{-29}(T/298)^{-2.96\pm0.09} \text{ cm}^6 \text{ molecule}^{-2} \text{ s}^{-1} \quad (24)$$

$$k_{1,inf} = (3.9 \pm 1.1) \times 10^{-11}(T/298)^{-1} \text{ cm}^3 \text{ molecule}^{-1} \text{ s}^{-1} \quad (25)$$

$$F_{cent,1} = 1.28 \exp(-389/T) - 0.62 + \exp(-T/331) \quad (26)$$

$$k_{2,tri} = (9.02 \pm 0.40) \times 10^{-29}(T/298)^{-3.36\pm0.11} \text{ cm}^6 \text{ molecule}^{-2} \text{ s}^{-1} \quad (27)$$

$$k_{2,inf} = (5.0 \pm 1.3) \times 10^{-11}(T/298)^{-1} \text{ cm}^3 \text{ molecule}^{-1} \text{ s}^{-1} \quad (28)$$

$$F_{cent,2} = 1.26 \exp(-305/T) - 0.60 + \exp(-T/271) \quad (29)$$

The falloff curves themselves can be used as an additional test on the value of the bond energy in $SiH_3-NO$. The parameter that is the most coupled to the bond energy is the weak collision efficiency parameter. Using $E_0$ as a fitting parameter with $\beta_c$ between 0.1 and 0.2 leads to $E_0 = 148-163$ kJ $mol^{-1}$. (The higher value in $E_0$ corresponds to the lower value in $\beta_c$.)

### Thermodynamic Functions

The thermodynamic functions of the reactants and products of reactions 1 and 2 were calculated using *ab initio* structures and scaled (factor 0.893) vibrational frequencies (HF/6-31G*).[10] These results are summarized in Tables 5 and 6 and in coefficients of NASA polynomials[45] in Table 7. The torsional motion in $SiH_3NO$ ($SiD_3NO$) was treated as a hindered internal rotation with a three-cycle sinusoidal potential. The barriers were calculated from the torsional frequencies under the assumption of a 3-fold sinusoidal potential. The reduced moments of inertia for the internal rotation and the contributions to the thermodynamic functions were calculated using the approach and tables of Pitzer and Gwinn.[46] The parameters used in the calculations are listed in the footnotes to the tables. The JANAF[28] data were used to obtain the coefficients of the NASA polynomials for NO.

### Discussion

Both reactions 1 and 2 are in the pressure falloff region significantly far from the true low-pressure limit. The pressure

dependence of the rate constants of reactions 1 and 2 is consistent with the $SiH_3-NO$ bond energy obtained in the equilibrium measurements. This value ($DH°_{298}(H_3Si-NO) = 158.9 \pm 4.0$ kJ mol$^{-1}$) is in fair agreement with the *ab initio*−BAC theoretical calculations ($DH°_{298}(H_3Si-NO) = 149.9$ kJ mol$^{-1}$. The discrepancy (9 kJ mol$^{-1}$), however, is much smaller than the discrepancy between the theoretical value and the previous estimates (*ca.* 30 kJ mol$^{-1}$) and can be assigned to the joint experimental uncertainty of the current experimental measurements and the accuracy of the BAC approach in application to Si-containing compounds.[47]

The bond energy in silylnitrosyl (158.9 kJ mol$^{-1}$) can be compared with the bond energy in trimethylsilylnitrosyl (190.2 kJ mol$^{-1}$ [10]). Therefore, substitution of hydrogen atoms by methyl groups leads to strengthening of the Si−N bond. The strengthening effect of methylation on Si−H bond has previously been observed and rationalized in terms of relative electronegativities of Si and C atoms[9,48]

**Acknowledgment.** This research was supported by the National Science Foundation, Chemistry Division, under Grant CHE-9102038. The authors express their gratitude to Dr. David B. Beach, who kindly provided $SiH_3I$ and $SiD_3I$.

## References and Notes

(1) Jasinski, J. M.; Meyerson, B. S.; Scott, B. A. *Annu. Rev. Phys. Chem.* **1987**, *38*, 109.

(2) Jasinski, J. M.; Gates, S. M. *Acc. Chem. Res.* **1991**, *24*, 9.

(3) Kapoor, V. J.; Stein, H. J. *Silicon Nitride Thin Insulating Films*; Symposium Proceedings; The Electrochemical Society: Pennington, NJ, 1983; Vol. 83-8.

(4) Belyi, V. I.; Vasilyeva, L. L.; Ginovker, A. S.; Gritsenko, V. A.; Repinsky, S. M.; Sinitsa, S. P.; Smirnova, T. P.; Edelman, F. L. *Silicon Nitride in Electronics*; Materials Science Monographs; Elsevier: Amsterdam, 1988; Vol. 34.

(5) Galasso, F. S.; Veltri, R. D.; Croft, W. J. *Am. Ceram. Soc. Bull.* **1978**, *57*, 453.

(6) Gebhardt, J. J.; Tanzilli, R. A.; Harris, T. A. *J. Electrochem. Soc.* **1976**, *123*, 1578.

(7) Jasinski, J. M.; Becerra, R.; Walsh, R. *Chem. Rev.* **1995**, *95*, 1203.

(8) Seetula, J. A.; Feng, Y.; Gutman, D.; Seakins, P. W.; Pilling, M. J. *J. Phys. Chem.* **1991**, *95*, 1658.

(9) Kalinovski, I. J.; Gutman, D.; Krasnoperov, L. N.; Goumri, A.; Yuan, W.-J.; Marshall, P. *J. Phys. Chem.* **1994**, *98*, 9551.

(10) Krasnoperov, L. N.; Niiranen, J. T.; Gutman, D.; Melius, C. F.; Allendorf, M. D. *J. Phys. Chem.* **1995**, *99*, 14347.

(11) Sugawara, K.; Katanaga, T.; Takeo, H.; Matsumara, C. *Chem. Phys. Lett.* **1989**, *157*, 309.

(12) Loh, S. K.; Jasinski, J. M. *J. Chem. Phys.* **1991**, *95*, 4914.

(13) Nay, M. A.; Woodall, G. N. C.; Strausz, O. P.; Gunning, H. E. *J. Am. Chem. Soc.* **1965**, *87*, 179.

(14) Kamaratos, E.; Lampe, F. W. *J. Phys. Chem.* **1970**, *74*, 2267.

(15) Marshall, P. *Chem. Phys. Lett.* **1993**, *201*, 493.

(16) Chasovnikov, S. A.; Gratsa, E. V.; Krasnoperov, L. N. Paper 142, presented at the 201st American Chemical Society Meeting, Atlanta, GA, April 1991.

(17) Slagle, I. R.; Gutman, D. *J. Phys. Chem.* **1986**, *90*, 2987.

(18) Slagle, I. R.; Gutman, D. *J. Am. Chem. Soc.* **1985**, *107*, 5342.

(19) Capellos, C.; Bielski, B. H. *Kinetic Systems*; Wiley-Interscience: New York, 1972.

(20) Moore, J. W.; Pearson, R. G. *Kinetics and Mechanism*, 3rd ed.; Wiley: New York, 1981; Chapter 8.

(21) Slagle, I. R.; Bernhardt, J. R.; Gutman, D. *Chem. Phys. Lett.* **1988**, *146*, 180.

(22) Krasnoperov, L. N.; Nosov, V. V.; Baklanov, A. V.; Panfilov, V. N. *Khim. Fiz.* **1988**, *7*, 528.

(23) Niiranen, J. T.; Gutman, D.; Krasnoperov, L. N. *J. Phys. Chem.* **1992**, *96*, 5881.

(24) *Handbook of Chemistry and Physics*, 53rd ed.; Weast, R. C., Ed.; The Chemical Rubber Co.: Cleveland, OH, 1972.

(25) Lias, S. G.; Bartmess, J. E.; Liebmann, J. F.; Holmes, J. L.; Levin, R. D.; Mallard, W. G. *Gas Phase Ion and Neutral Thermochemistry*; Lide, D. R., Ed.; *J. Phys. Chem. Ref. Data* **1988**, *17* (Suppl. No. 1).

(26) Benson, S. W. *Thermochemical Kinetics*, 2nd ed.; Wiley: New York, 1976.

(27) Morgan, C. A.; Pilling, M. J.; Tulloch, J. M.; Ruiz, R. P.; Bayes, K. D. *J. Chem. Soc., Faraday Trans. 2* **1982**, *78*, 1323.

(28) Chase, M. W., Jr.; Davies, C. A.; Downey, J. R., Jr.; Frurip, D. J.; McDonald, R. A.; Syverud, A. N. *JANAF Thermochemical Tables*, 3rd ed.; *J. Phys. Chem. Ref. Data* **1985**, *14* (Suppl. No. 1).

(29) Hudgens, J. W. Table VI in: *J. Phys. Chem.* **1991**, *95*, 1658.

(30) Davies, J. W.; Green, N. J. B.; Pilling, M. J. *J. Chem. Soc., Faraday Trans.* **1991**, *87*, 2317.

(31) Masanet, J.; Calarp, F.; Jemi-Alade, A. A.; Lightfoot, P. D.; Lesclaux, R.; Rayez, M. T. *J. Phys. Chem.* **1993**, *97*, 3237.

(32) Smith, I. W. M. *Int. J. Chem. Kinet.* **1984**, *16*, 423.

(33) Wallington, T. J.; Maricq, M. M.; Ellermann, T.; Nielsen, O. J. *J. Phys. Chem.* **1991**, *96*, 982.

(34) Vakhtin, A. B.; Petrov, A. K. *Chem. Phys.* **1991**, *149*, 427.

(35) Kaiser, E. W. *J. Phys. Chem.* **1993**, *97*, 11681.

(36) Pagsberg, P.; Munk, J.; Anastasi, C.; Simpson, V. J. *J. Phys. Chem.* **1989**, *93*, 5162.

(37) Masanet, J.; Calarp, F.; Ley, L.; Lesclaux, R. *Chem. Phys.* **1992**, *160*, 383.

(38) Troe, J. *J. Chem. Phys.* **1977**, *66*, 4758.

(39) Gardiner, W. C., Jr.; Troe, J. Rate Coefficients of Thermal Dissociation, Isomerization, and Recombination Reactions. In *Combustion Chemistry*; Gardiner, W. C., Jr., Ed.; Springer-Verlag: New York, 1984; pp 173−196.

(40) Hippler, H.; Troe, J.; Wendelken, H. J. *J. Chem. Phys.* **1983**, *78*, 6709.

(41) Reid, R. C.; Sherwood, T. K. *The Properties of Gases and Liquids*; McGraw-Hill: New York, 1958.

(42) Chasovnikov, S. A.; Krasnoperov, L. N. *Kinet. Catal. (Engl. Transl.)* **1990**, *31*, 1125.

(43) Gilbert, R. G.; Luther, K.; Troe, J. *Ber. Bunsen-Ges. Phys. Chem.* **1983**, *87*, 169.

(44) Hippler, H.; Troe, J. Recent Direct Studies of Collisional Energy Transfer in Vibrationally Highly Excited Molecules in the Ground Electronic State. In *Bimolecular Collisions*; Ashfold, M. N. R., Baggott, J. E., Eds.; The Royal Society of Chemistry: London, 1989; pp 209−262.

(45) Gordon, S.; McBride, B. D. NASA Report NASA-SP-273, 1971.

(46) Pitzer, K. S.; Gwinn, W. D. *J. Chem. Phys.* **1942**, *10*, 428.

(47) Ho, P.; Melius, C. F. *J. Phys. Chem.* **1990**, *94*, 5120.

(48) Ding, L.; Marshall, P. *J. Am. Chem. Soc.* **1993**, *115*, 2539.